JACS
JOURNAL OF THE AMERICAN CHEMICAL SOCIETY
Article
pubs.acs.org/JACS

A Core/Satellite Multifunctional Nanotheranostic for in Vivo Imaging and Tumor Eradication by Radiation/Photothermal Synergistic Therapy

Qingfeng Xiao,[†] Xiangpeng Zheng,[‡] Wenbo Bu,*[,†] Weiqiang Ge,[‡] Shengjian Zhang,[§] Feng Chen,[†] Huaiyong Xing,[†] Qingguo Ren,[‡] Wenpei Fan,[†] Kuaile Zhao,[§] Yanqing Hua,[‡] and Jianlin Shi*[,†]

[†]State Key Laboratory of High Performance Ceramics and Superfine Microstructures, Shanghai Institute of Ceramics, Chinese Academy of Sciences, Shanghai, 200050, P.R. China

[‡]Department of Radiation Oncology, Shanghai Huadong Hospital, Fudan University, Shanghai, 200040, P.R. China

[§]Department of Radiology, Shanghai Cancer Hospital, Fudan University, Shanghai, 200032, P.R. China

Supporting Information

ABSTRACT: To integrate photothermal ablation (PTA) with radiotherapy (RT) for improved cancer therapy, we constructed a novel multifunctional core/satellite nanotheranostic (CSNT) by decorating ultrasmall CuS nanoparticles onto the surface of a silica-coated rare earth upconversion nanoparticle. These CSNTs could not only convert near-infrared light into heat for effective thermal ablation but also induce a highly localized radiation dose boost to trigger substantially enhanced radiation damage both *in vitro* and *in vivo*. With the synergistic interaction between PTA and the enhanced RT, the tumor could be eradicated without visible recurrence in 120 days. Notably, hematological analysis and histological examination unambiguously revealed their negligible toxicity to the mice within a month. Moreover, the novel CSNTs facilitate excellent upconversion luminescence/magnetic resonance/computer tomography trimodal imagings. This multifunctional nanocomposite is believed to be capable of playing a vital role in future oncotherapy by the synergistic effects between enhanced RT and PTA under the potential trimodal imaging guidance.

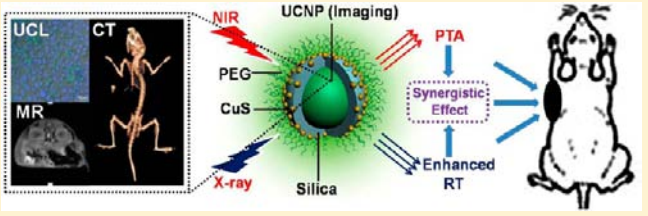

INTRODUCTION

As a minimally invasive and harmless therapy approach, near-infrared (NIR) laser induced-photothermal ablation has gained a rapid development recently due to the minor attenuation and favorable biosafety of NIR in tissues. Numerous photothermal agents especially nanomaterials with strong absorbance of NIR laser have been extensively explored to increase the photothermal conversion efficiency and correspondingly, enhance the thermal lethality in subcutaneous tumors.[1−7] Among them, CuS nanoparticles (NPs) attracted particular attention because of their low cost, low cytoxicity, and high photothermal conversion efficiency.[8−11]

However, though highly efficient photothermal agents have been employed, the difficulties in controlling deep-located tumors still remain as the intrinsic shortcoming of optical therapy because of the inevitable depth-dependent decline of laser intensity.[12] Comparatively, radiotherapy (RT) uses high-energy, highly focused radiation rays (generally X-ray and γ-ray) as virtual "knives" to kill cancer cells with no depth restriction and invasiveness. Moreover, a local radiation dose could be flexibly and effectively amplified by the introduction of high-Z nanomaterials as radiosensitizers.[13−19] Among numerous intensifiers, the Yb-based upconversion nanoparticle (UCNP) is anticipated to be a very competent candidate since it can not only enhance radiation dose due to the presence of high Z rare earth elements but also provide multimodal imaging functions.[20,21] Remarkably, the use of these NPs will facilitate the collection of detailed and exact information of a lesion, such as the location and outline of tumors. More importantly, by loading these intensifiers into a deep-located tumor to conduct nanomaterial-enhanced RT, a greater local radiation dose could be generated and concentrated on a tumor than that from RT alone without additional radio-toxicity to surrounding normal tissues.

Therefore, the combination of nanomaterials-enhanced RT with photothermal ablation (PTA) will offset the disadvantage of PTA alone on the deep-seated tumor. More excitingly, PTA used as hyperthermia can in turn serve as an effective strategy for radiotherapy sensitization and bring a strong synergistic effect to conquer the inherent drawbacks of RT: (1) A high RT therapeutic effect cannot be achieved on S-phase cells which are considered as the least radiation-sensitive ones in the cell replication cycle and hypoxic cells with a serious negative effect on the tumor's response to RT. Encouragingly, all these radio-resistant cells are very sensitive to the lethal effects of hyperthermia;[22,23] (2) An appropriate level of hyperthermia could increase intratumoral blood flow and subsequently

Received: May 17, 2013
Published: August 7, 2013

   dx.doi.org/10.1021/ja404985w | J. Am. Chem. Soc. 2013, 135, 13041−13048

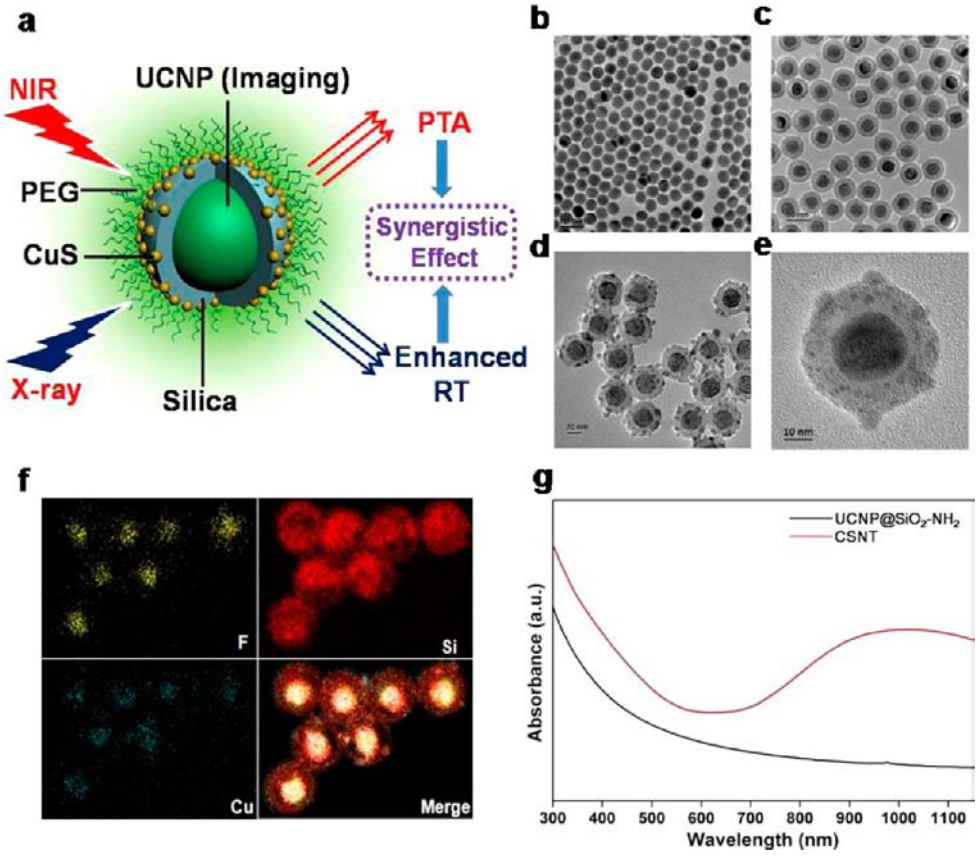

Figure 1. Characterization of the CSNTs. (a) Schematic of a CSNT for enhanced RT/PTA synergistic therapy. UCNP cores are used to enlarge the local radiation dose for the enhanced RT, and CuS satellites are responsible for converting the 980 nm laser into heat for PTA. The combination of PTA and CSNT-enhanced RT could give rise to a strong synergistic effect and then construct a RT/PTA synergistic system. (b–e) Transmission electron microscopic images of (b) UCNP, (c) UCNP@SiO_2–NH_2, and (d, e) CSNT at different magnifications. (f) Element mappings (F, Si, and Cu, respectively) of CSNTs. (g) UV–vis–NIR absorption spectrum of UCNP@SiO_2–NH_2 and CSNT.

improve oxygenation status in the tumor, which will consequently result in the considerably increased cell sensitivity to radiation therapy;[24] (3) The repair of the nonlethal damage from RT might be effectively suppressed by hyperthermia.[25] Therefore, the integration of PTA and nanomaterials-enhanced RT could effectively combine mutual advantages together while offsetting their corresponding disadvantages, generate a strong synergistic effect, and then give rise to much greater antitumor efficacy than the two treatments alone or even the projected sum of the two treatments. However, how to construct such a composite system efficiently integrating the two therapeutic modalities remains a great challenge.

In this study, we developed a new type of multifunctional nanotheranostic with silica-coated rare-earth upconversion nanoparticles ($NaYbF_4$: 2%Er^{3+}/20%Gd^{3+}@SiO_2–NH_2) as the core and ultrasmall CuS NPs as the satellites for synergistic RT/PTA therapy, which has not been investigated to date. Such core/satellite nanotheranostics (CSNTs) of 45 nm in diameter on average could produce significant amounts of cytotoxic heat upon 980 nm laser excitation and simultaneously could serve as radiosensitizers to generate dose-enhancement effects of RT by the high Z elements (Yb, Gd, and Er) contained in UCNPs, which would result in remarkable *in vitro* cell damage and *in vivo* tumor regression. Complete eradication of tumor tissue without late recurrence could be achieved by the RT/PTA synergistic therapeutic effect. A simulation experiment demonstrates that CSNT-enhanced RT could assist PTA in eliminating deep-seated tumors. The *in vivo* systemic toxicity of CSNTs examined by hematological and histological analysis in major organs did not show any signs of adverse effect to mice within one month. Furthermore, UCNP itself as a natural imaging nanoprobe endows CSNT with several imaging modalities,[20,21,26–29] such as upconversion luminescence (UCL), magnetic resonance (MR), and computer tomography (CT), which indicates the great potential for an early cancer diagnosis and multimodal image-guided tumorous therapeutic alliance in the future.

EXPERIMENT SECTION

In Vitro PTA. 3-(4,5-Dimethylthiazol-2-yl)-2, 15-diphenyltetrazolium bromide (MTT) assay was used to quantitatively investigate photothermal cytotoxicity of CSNTs in vitro. Hela cells were incubated with different concentrations of 0, 150, 300, and 600 μg/mL of CSNT for 4 h, and then excess CSNTs were removed by PBS washing. Then, a 980 laser (1.5 W/cm^2) was used to irradiate the cells for 5 min, and the cells were then incubated for another 20 h. Cell viability was determined by MTT assay.

In Vitro CSNT-Enhanced RT. Hela cells were seeded into a 96-well cell-culture plate at 10^5/well and then incubated for 24 h at 37 °C under 5% CO_2. DMEM solutions of CSNTs with different concentrations of 0, 150, 300, and 600 μg/mL were added to the wells and coincubated for another 4 h. Excess CSNTs were removed by PBS washing, followed by 6 Gy of X-ray radiations and incubated 20 h again. Cell viability was determined by MTT assay.

In Vitro CSNT-Enhanced RT/PTA Synergistic Effect. DMEM solutions of CSNTs at the concentrations of 600 μg/mL were

dx.doi.org/10.1021/ja404985w | J. Am. Chem. Soc. 2013, 135, 13041–13048

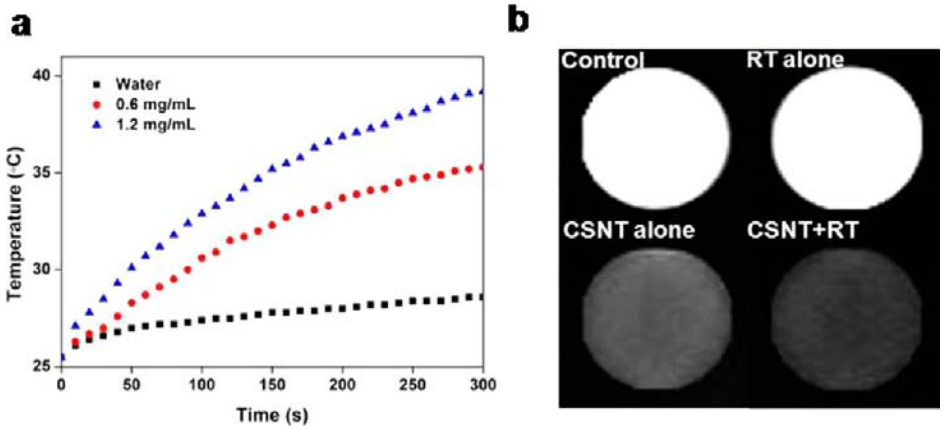

Figure 2. (a) Concentration-dependent temperature increases of CSNT solutions (980 nm, 1.5 W/cm^2, 5 min). (b) The X-ray radiation dose-enhancement effect was assessed by polymer gel experiments. The variation of MRI-T_2 signal intensity was related to the change of radiation dose. RT experiments were conducted at the constant dose of 6 Gy.

coincubated with cells for 4 h at 37 °C under 5% CO_2, and then excess CSNTs were removed by PBS. Cells were exposed to the 980 laser (1.5 W/cm^2) for 5 min and incubated for 30 min (PTA treatment), followed by 6 Gy of X-ray radiations in 5 min (RT treatment) and incubation again for 20 h. Cell viability was determined by MTT assay. The projected additive value was calculated by multiplying the viability of cells from PTA by the viability of the cells with CSNT-enhanced RT treatment.

In Vivo RT/PTA Synergistic Therapy on a Subcutaneous Tumor Model Injected with CSNTs. All animal experiments were conducted under protocols approved by the Fudan University Laboratory animal center. Tumors were induced by subcutaneous implantation of 1.5×10^6 4T$_1$ cells suspended in 150 μL of phosphate buffered saline (PBS) into the right shoulder of each female Balb/c mouse. When the tumor volume reached $\approx$ 75 mm^3, the tumor therapy was performed as follows: (1) PBS alone; (2) CSNT alone; (3) NIR alone; (4) RT alone; (5) CSNT + RT; (6) CSNT + NIR; (7) CSNT + RT + NIR. A dosage of CSNT (1.4 mg/mL, 150 μL) was intratumorally administrated into the mice in group 2, 5, 6, and 7. After 1 h, the mice received the treatment of RT for the group 5 and the irradiation of 980 nm laser for 8 min for the group 6 in the tumor site, respectively. The CSNT-loaded mice in group 7 received the RT treatment at 30 min after the exposure of 980 nm laser. Tumor sizes were measured every 2 days after treatment using a vernier caliper, and the whole process lasted 16 days. Tumor growth inhibition (TGI) was calculated with the formula: TGI (%) = $100 \times (R_1 - R_n)/R_1$, where R_1 is the relative tumor volume of the group 1 and R_n is the relative tumor volume of the nth group. Another five groups of mice (CSNT; RT; CSNT+RT; CSNT+NIR; CSNT+RT+NIR) were subject to NIR/RT treatments similar to the above experiment 3 h after intravenous injection (21.4 mg/mL, 150 μL). The tumor volume of each mouse was also measured by vernier caliper every other day.

RESULTS AND DISCUSSION

Synthesis and Characterization of CSNT. This multifunctional CSNT was prepared by a simple water-in-oil reverse microemulsion strategy and subsequent electrostatic adsorption technique between positively charged UCNP@SiO_2-NH_2 and negatively charged citrate-stabilized CuS NPs (section 1 in the Supporting Information). In this structure, the UCNP inner core is mainly responsible for augmenting the radiation dose of RT owing to the high Z value rare earth elements (Yb, Gd, and Er) and UCL/MR/CT trimodal imaging while CuS satellites were employed as photothermal agents to increase photothermal conversion efficacy (Figure 1a). The poly(ethylene glycol) (PEG) was finally grafted to prevent aggregations among the particles and impart excellent water-solubility and biocompatibility.[10,30−32] As indicated in the transmission electron microscopy (TEM) images, the products obtained after each synthetic step show an excellent dispersity and uniformity in both morphology and dimension with an ultimate average diameter of 45 nm (Figure 1b−d and Figure S1a,b in the Supporting Information). The core−satellite structure could be clearly seen in the high-magnification TEM and STEM (scanning transmission electron microscopy) images (Figure 1e and Figure S1c in the Supporting Information). Energy dispersive spectroscopic (EDS) element mappings of F, Si, and Cu were further performed to investigate the distribution of various components (Figure 1f). The results show that CuS satellites could be firmly attached and well distributed on the surface of UCNP@SiO_2−NH_2 core owing to the beneficial electrostatic adsorption. The appearance of the broad absorption peak, the increase in the hydrodynamic diameter (from 58.8 to 74.9 nm) and the decline of zeta potentials (from +28.6 mV to −10.5 mV) in the preparation process prove the effective adherence of the CuS NPs on the cores (Figure 1g and Figure S1d,e in the Supporting Information).[10,31,32] The variations of the characteristic functional groups in FT-IR spectra are also indicative of the successful silica coating and PEG modification (Figure S1f in the Supporting Information).[31] The luminescence spectrum displays three characteristic emission peaks located at 519 nm ($^2H_{11/2}\rightarrow{}^4I_{15/2}$), 538 nm ($^4S_{3/2}\rightarrow{}^4I_{15/2}$), and 652 nm ($^4F_{9/2}\rightarrow{}^4I_{15/2}$) from CSNTs under 980 nm laser irradiation (Figure S1g in the Supporting Information), providing a favorable basis for the cellular localization. The Yb/Si/Cu weight ratio was ultimately determined by inductively coupled plasma atomic emission spectroscopy (ICP−AES) to be 1:0.7:0.59.

In Vitro CSNT-Enhanced RT/PTA Synergistic Therapy. Through the adherence of CuS satellites, CSNTs are endowed with the distinct photothermal conversion performance. As shown in the temperature variation curve, the temperature increased remarkably when CSNT solution was exposed to 980 nm laser (power: 1.5 W/cm^2) for 5 min, in contrast with only a slight temperature variation in the pure water (Figure 2a), suggesting that the NIR laser had been transformed into heat by the CSNTs. Moreover, the impact of CSNT on the radiation dose was investigated using MRI-mediated polymer gels dosimetry.[33] It was found that the two gel groups with CSNTs displayed visible gray (T_2-signal) due to the presence of Gd^{3+} while the darker gray appears in the CSNT plus RT

dx.doi.org/10.1021/ja404985w | J. Am. Chem. Soc. 2013, 135, 13041−13048

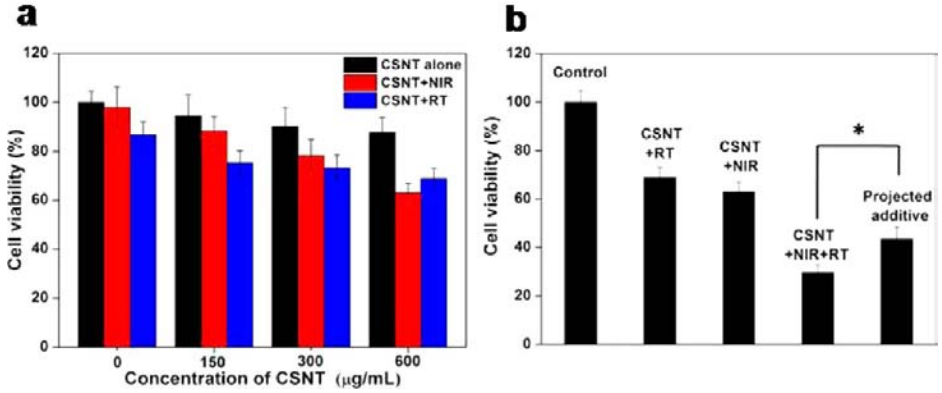

Figure 3. (a) Quantitative analysis of the cell viability with CSNTs at varied concentrations with or without NIR-laser irradiation and RT. (b) Synergistic therapeutic effect of Hela cells that have taken up CSNTs subjected to RT, PTA, and the combined RT/PTA treatments. The projected additive value is calculated by multiplying the cell viability of CSNT+RT group by the cell viability of the CSNT+NIR group. Statistical analysis was performed using the Student's two-tailed *t* test (*$P < 0.05$). All PTA experiments on the cellular level were performed under the same condition (980 nm, 1.5 W/cm^2, 5 min). RT experiments were conducted at the constant dose of 6 Gy.

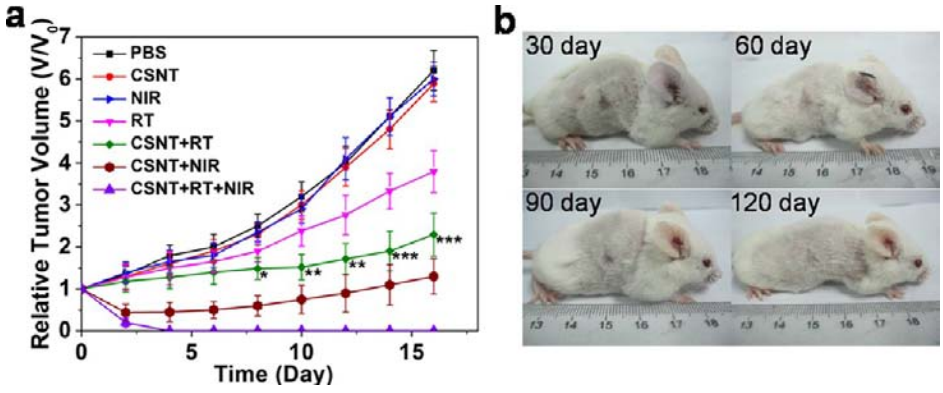

Figure 4. In vivo CSNT-enhanced RT/PTA synergistic therapeutic effects of tumor-bearing mice intratumorally injected with CSNTs. (a) Time-dependent tumor growth curves of different groups of mice with various treatments. In all experiments, the power density of 980 nm NIR-laser and the radiation dose used for RT were kept constant at 1.5 W/cm^2 and 6 Gy, respectively. The significant difference between groups 4 and 5 at day 8 and beyond after the treatments widened gradually, indicating the effectiveness of CSNT-enhanced RT. Statistical analysis was performed using the Student's two-tailed *t* test (*$P < 0.05$, **$P < 0.01$ and ***$P < 0.001$). (b) The photographs of mice in 30, 60, 90, and 120 days of treatment (group 7) showing the complete eradication of the tumor and no visible recurrences of the tumors in at least 120 days.

(Figure 2b), indicating that the presence of CSNTs in gels contributed significantly to the radiation energy deposition and subsequent dose enhancement. On the basis of the above satisfactory results, we further assessed the applicability of CSNTs as photothermal agents and radiosensitizers on a cellular level using 3-(4,5-dimethylthiazol-2-yl)-2,15-diphenyl-tetrazolium bromide (MTT) assay. Quantitative evaluation showed that more than 87% of the cells treated with CSNTs alone at a high concentration of 600 μg/mL are still alive. However, the percentage greatly declines to 63% after the cells received irradiation of the nontoxic NIR-laser (980 nm, 1.5 W/cm^2, 5 min). Likewise, after combinational treatments of CSNT (0.6 mg/mL) and RT, the cell viability dropped to 68.9% compared to 86.7% of RT alone. These results well demonstrate the suitability of CSNTs as efficient photothermal converters and radiosensitizers (Figure 3a). To illustrate the presence of the synergistic effect between RT and PTA, we treated the cancer cells engulfing CSNTs by 980 nm laser irradiation for 5 min prior to RT. It was found that cell viability could substantially decrease to 29.6%, which was 53% lower than that of PTA alone, 57% lower than that of CSNT-enhanced RT alone, and even 31.8% lower than the projected additive value (43.4%, *$P = 0.0401$),[34] strongly confirming the considerable CSNT-enhanced RT/PTA synergistic effect in vitro (Figure 3b).

In Vivo CSNT-Enhanced RT/PTA Synergistic Therapy. Encouraged by the favorable *in vitro* results, we further investigated the feasibility of CSNTs in *in vivo* RT/PTA synergistic cancer therapy by intratumoral injection. Herein, Balb/c mice bearing subcutaneous 4T$_1$ murine breast cancer tumors were randomly divided into seven groups ($n = 7$) receiving specific treatments as follows: (1) PBS alone; (2) CSNT alone; (3) NIR alone; (4) RT alone; (5) CSNT + RT; (6) CSNT + NIR; (7) CSNT + RT + NIR. The animal survival status and the variation of relative tumor volume were monitored over time (Figure S2 in the Supporting Information and Figure 4a). At 16 days after treatment, comparable growth rates were found in groups 1, 2, and 3 with relative tumor volume (V/V$_0$) of 6.2 ± 0.47, 5.9 ± 0.43, and 6.0 ± 0.4, respectively, indicating the negligible effect by the single utilization of either CSNT or NIR-laser (1.5 W/cm^2) on the progress of tumor growth (Table S1 in the Supporting Information). Remarkably, the tumor in group 6 shows a serious burn and a considerable tumor growth inhibition (TGI) of 79% (V/V$_0$ = 1.3 ± 0.42), reflecting the potential of CSNTs as photothermal agents in vivo, which is additionally confirmed

dx.doi.org/10.1021/ja404985w | J. Am. Chem. Soc. 2013, 135, 13041−13048

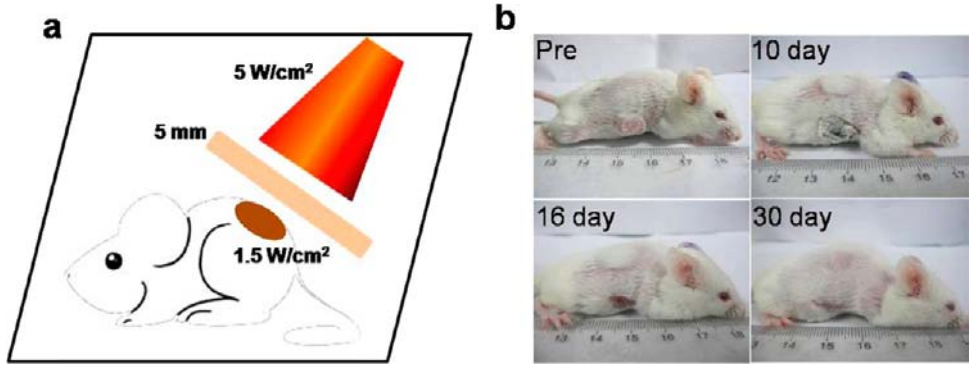

Figure 5. Simulation experiments of treating interior tumors deep under the skin with PTA alone. (a) Schematics of experiment design *in vivo*. (b) Representative gross photographs of the mouse receiving a single intratumoral injection (1.4 mg/mL, 150 μL) at various time points (10, 16, and 30 day) after irradiation of 980 nm laser (8 min) at the power density of 5 W/cm^2.

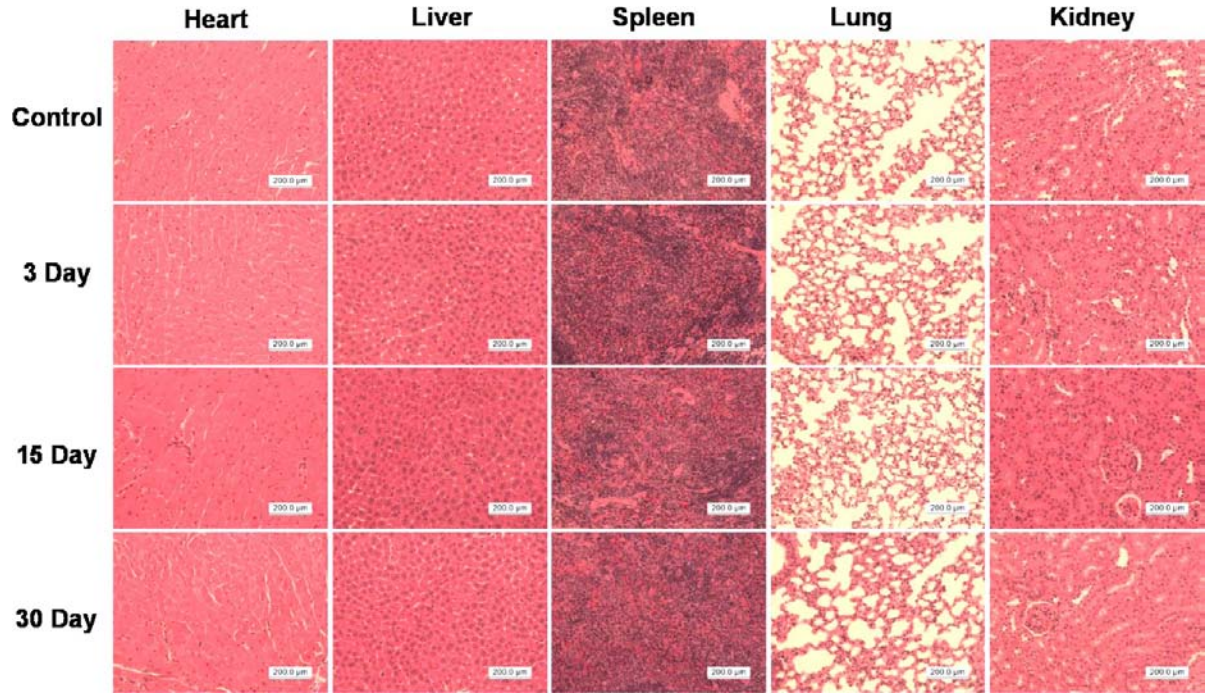

Figure 6. H&E-stained tissue sections from mice to monitor the histological changes in liver, spleen, heart, kidney, and lung of mice receiving single intravenous injection of PBS (control, 150 μL) or 10.5 mg/kg (150 μL for each mouse) of CSNT followed by dissections in 3, 15, and 30 days postinjection.

by the infrared thermal mappings (Figure S3 in the Supporting Information). With respect to RT, the distinct difference between groups 4 and 5 reveals that compared to RT alone (group 4, TGI = 38.7%, V/V_0 = 3.8 ± 0.5), the combination of RT and CSNTs could achieve more significant tumor growth control (group 5, TGI = 62.9%, V/V_0 = 2.3 ± 0.51, ***P = 0.0004 versus group 4), demonstrating that CSNTs played an important role in increasing the efficacy of RT. To prove the synergistic effect between CSNT-enhanced RT and PTA in vivo, we treated tumor-bearing and CSNT-injected mice using 980 nm laser and RT successively (group 7). As shown, the tumor was thoroughly eradicated in four days without later recurrence during a prolonged period up to 120 days (Figure 4b). By comparison, the tumor in CSNT+RT (group 5) only exhibited a decelerated growth pattern rather than evident shrinkage, probably attributable to the limited radiation dose enhancement and the existence of radio-resistant cells. The PTA (group 6) also resulted in only about a half tumor contraction in four days compared to the original tumor volume. On the basis of these obvious discrepancies, it is assumed that PTA could initially kill some superficial cancer cells as well as radio-resistant hypoxic cells and S-phase cells, but in the meantime also benefit the oxygenation of the residual cells, leaving them relatively radio-sensitive and then easily killed by RT.[22−24,35] Therefore, the synergistic effect could be ultimately brought into full play, resulting in the complete eradication of the tumor. Moreover, histological changes of tumor tissues collected at three days after the corresponding treatments were examined by hematoxylin and eosin (H&E) staining. The results show that treatment with CSNT + NIR and CSNT + RT could cause more evident tumor damage, such as irregular widening of intercellular space, than corresponding NIR-laser alone and RT alone. The most significant tumor destruction was achieved by the treatment of CSNT + RT + NIR, consistent with the inhibition results of tumor growth rate, further demonstrating the distinct CSNT-enhanced RT/

dx.doi.org/10.1021/ja404985w | J. Am. Chem. Soc. 2013, 135, 13041−13048

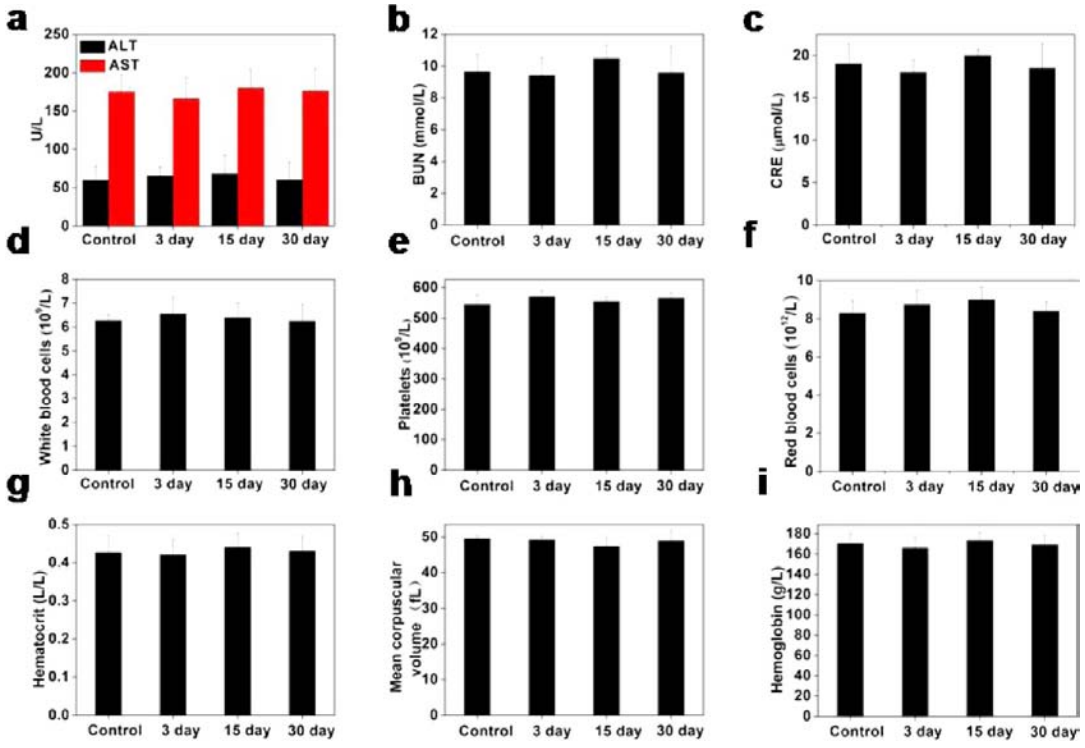

Figure 7. (a) The blood levels of alanine aminotransferase (ALT) and aspartate aminotransferase (AST) as liver function markers. (b) Blood urea nitrogen (BUN) and (c) creatinine (CRE) levels in the blood marking kidney functions. The two markers show no significant difference, demonstrating little side effect of CSNTs on liver and kidney. (d–i) The complete blood panel data from healthy control and treated mice: (d) white blood cells, (e) platelets, (f) red blood cells, (g) hematocrit, (h) mean corpuscular volume, (i) hemoglobin.

PTA synergistic effect (Figure S4 in the Supporting Information). The potential various treatment-induced in vivo side effects, a great concern in the biomedical field, were also assessed by measuring the weight of mice in each group every two days until the end of the experiments. It was found that the body weight of mice in groups 4, 5, and 7 slightly declined within the initial four days after the treatments, then recovered and kept gradually increasing. In 16 days, neither significant weight loss relative to the original weight nor any abnormal behavior was observed in all groups (Figure S5 in the Supporting Information), indicating that the treatments had not brought about a significant in vivo side effect, which was very essential for ensuring a good living standard.

Simulation Experiment. To simulate the treatment of interior tumors deep under the skin, we covered tumors with a 5-mm thick pork tissue and meanwhile kept the NIR-laser power density at 1.5 W/cm^2 on the surface of the tumor by tuning the power density of the incident laser on the outer side of pork tissue to be as high as 5 W/cm^2. This shows a more than 3-fold attenuation of laser intensity after penetrating 5-mm thick tissue (Figure 5a). Subsequently, the pork was removed and the follow-up experiment was carried out in the same way as that in group 6 except for the increased power density (maintained at 5 W/cm^2). Under this condition, we found the tumor could be thoroughly eliminated (Figure 5b), which was in striking contrast with the partial damage of the tumor in group 6 under 1.5 W/cm^2. This demonstrates that, in spite of providing a good therapeutic effect to the subcutaneous tumor under the presence of CSNTs, the power density of 5 W/cm^2 of PTA alone is still not sufficient to treat the interior tumor about 5 mm under the skin due to the inevitable depth-dependent power attenuation. However, inspired by the foregoing satisfactory anticancer results in group 7, it is expected with confidence that through the introduction of CSNT-enhanced RT, the complete eradication of the interior tumor tissue that is situated up to 5 mm under the skin could be achieved at an incident laser power density of 5 W/cm^2, which throws light on the potential of CSNT-enhanced RT/PTA synergistic therapy to deal with the deep-seated tumors. The present demonstration indicates that though the under-skin depth here is only 5 mm, in the future, the concept of the synergistic therapy will be highly favorable in the fight against interior tumors.

Toxicity assessment *in Vivo*. To investigate whether CSNT resulted in any detrimental effect, we further carried out hematoxylin and eosin (H&E) staining, blood chemistry, and complete blood panel analysis for healthy mice 3, 15, and 30 days after a single intravenous injection of CSNTs at a dosage of 10.5 mg/kg (150 μL for each mouse). Fortunately, no noticeable tissue damage and adverse effect to various organs could be observed from the hematoxylin and eosin (H&E) staining (Figure 6). There is also no visible significant variation of blood parameters over time between the treatment groups and the control in blood chemistry and complete blood panel analysis (Figure 7). These results offer a preliminary proof that CSNTs at the given dose hardly cause any *in vivo* toxicity effect.

UCL/CT/MR Trimodal Imaging. Cellular uptake experiments were performed to assess the ability of cellular uptake and applicability of CSNTs in UCL imaging. The results testify that CSNTs can be well taken up by endocytosis, gather in the cytoplasm, and emit strong fluorescence under excitation (Figure S6 in the Supporting Information). CT images were acquired using varied concentrations of CSNTs in deionized water and showed sharp signal enhancement at the increased

dx.doi.org/10.1021/ja404985w | J. Am. Chem. Soc. 2013, 135, 13041–13048

concentrations of CSNTs (Figure S7a in the Supporting Information). The feasibility of CSNTs as *in vivo* CT contrast agents was certified by the notable brightness difference between the treatment and control group in tumor regions (Figure S7b in the Supporting Information). T_1- and T_2-weighted MR images of CSNTs display the concentration-dependent brightening and darkening effects, respectively (Figure S8a in the Supporting Information). It should be pointed out that apart from the main role played by Gd, with seven unpaired electrons, in the increasing T_1-weighted MR contrast effect of CSNTs, the assistant effect from the CuS satellites ascribed to the presence of Cu^{2+} with one unpaired electron should not be neglected. This effect may be demonstrated by the concentration-dependent signal enhancement of the single CuS aqueous solution, as was first reported in this study (Figure S8b in the Supporting Information). The remarkable T_1- and T_2-weighted contrast enhancements in the tumor area evidence the capability of simultaneous T_1- and T_2-weighted imagings of CSNTs in vivo (Figure S9 in the Supporting Information).

To sum up, CSNTs could be an effective trimodal diagnostic tool from the cellular scale to the whole body scale, which may provide a promising platform for image-guided therapy in the future.

The Assessment of Potential Medical Application by Intravenous Administration. To be more close to practical application, we conducted in vivo tumor MR imaging studies by the intravenous injection of CSNTs. The results display distinguishable lighting and darkening effects in the tumor 1.5 h after injection, with the T_1- and T_2-weighted signal values increased by 29.1% and decreased by 17.5%, respectively (Figure S10 in the Supporting Information). This evidence verifies that CSNTs could be successfully delivered into a tumor by blood circulation via passive targeting for enhanced T_1- and T_2-weighted imagings.

Next, we extended the investigation to examine the CSNT-enhanced RT/PTA synergistic effect by intravenously injecting CSNTs. Actually, there have been many reports about cancer drug delivery via passive accumulation.[1,2,5,10,36] Here, our results show that the tumors of mice intravenously injected with CSNTs could be clearly suppressed by RT or NIR treatment, while the most significant inhibition was found on mice subjected to NIR and RT combinational treatment, which undoubtedly should be ascribed to the passive targeting of CSNTs in tumor tissue and the favorable RT/PTA synergistic effect (Figures S11, S12, and S13 and Table S2 in the Supporting Information). However, as expected, the complete elimination of a tumor could not be achieved by intravenous injection because of inadequate accumulation of the CSNTs in the tumor. This demonstrates the urgent demand to further improve and optimize the nanomaterials to be more favorable for their transformation into clinical applications.

CONCLUSION

A multifunctional nanotheranostics has been constructed as the first example of integrating nanomaterial-enhanced RT, PTA, and UCL/MR/CT trimodal imagings together. The in vitro and in vivo results show that (1) NIR laser could be absorbed by CSNTs and transferred into considerable amounts of local thermal energy for cancer cell ablation, showing the applicability of CSNTs as photothermal agents; (2) the presence of high Z elements (Yb, Gd, and Er) in CSNTs could cause a large local radiation dose-enhancement around the NPs, demonstrating that CSNTs could also be used as radiosensitizers; (3) the CSNTs integrating CuS NPs and UCNP by electrostatic adsorption act as highly efficient carriers for a strong RT/PTA synergistic effect, which makes a great contribution to the tumor eradication. Although such an excellent curative effect is established on the strategy of intratumoral injection, the concept of RT/PTA synergistic therapy has been undoubtedly confirmed to be highly efficient. More importantly, subsequent treatments by intravenous injection also show a very distinct therapeutic effect, which clearly demonstrates the future application potentials of the RT/PTA synergistic therapy of CSNTs; (4) UCL/MR/CT trimodal imagings could be simultaneously performed with this multifunctional nanotheranostic, which lay the groundwork for the image-guided therapy in the future. Moreover, no significant harm could be observed in both *in vitro* and *in vivo* toxicity studies, indicating its good biocompatibility. We believe that this research offers the first proof of concept for the integration of the nanomaterial-enhanced RT/PTA, together with UCL/MR/CT trimodal bioimagings. In the future, this integration is expected to produce a powerful platform for the multimodal image-guided therapeutic alliance with significant therapeutic effect.

More promising is that UCNP itself as a multifunctional matrix could play an important role in many detection and therapeutic protocols, such as intracellular sensing of temperature,[37] NIR-induced photodynamic (PDT),[36,38,39] and NIR-controlled drug release.[40−42] Alternatively, CuS nanoparticles alone could also achieve the integration of a diagnosis like photoacoustic tomography[32] and photothermal-induced intelligent drug delivery. Therefore, the further functionalization based on CSNTs could undoubtedly bring more attractive diagnosis and therapy strategies.

ASSOCIATED CONTENT

Supporting Information

Synthesis procedures for UCNP, UCNP@SiO_2−NH_2, and CSNT; materials characterization; and other supplementary figures. This material is available free of charge via the Internet at http://pubs.acs.org.

AUTHOR INFORMATION

Corresponding Author

wbbu@mail.sic.ac.cn; jlshi@mail.sic.ac.cn

Present Address

[⊥]1295 Ding-xi Road, Shanghai 200050, China.

Notes

The authors declare no competing financial interest.

ACKNOWLEDGMENTS

This work has been financially supported by the National Natural Science Foundation of China (Grant No.50823007, 50972154, 51132009, 51072212, 21172043, 51102259), the Shanghai Rising-Star Program (Grant No. 12QH1402500), the Nano Special Program of the Science and Technology Commission of Shanghai (Grant No.11 nm0505000), the Development Foundation for Talents of Shanghai (Grant No.2012035), the Young Investigator Fund of Fudan University (Grant No.EYF163006), and the Science and Technology Commission of Shanghai (Grant No.124119a0400).

REFERENCES

(1) Cheng, L.; Yang, K.; Chen, Q.; Liu, Z. *ACS Nano* **2012**, *6*, 5605.
(2) Liu, H.; Liu, T.; Wu, X.; Li, L.; Tan, L.; Chen, D.; Tang, F. *Adv. Mater.* **2012**, *24*, 755.
(3) Yang, K.; Xu, H.; Cheng, L.; Sun, C.; Wang, J.; Liu, Z. *Adv. Mater.* **2012**, *24*, 5586.
(4) Liu, Z.; Chen, K.; Davis, C.; Sherlock, S.; Cao, Q.; Chen, X.; Dai, H. *Cancer Res.* **2008**, *68*, 6652.
(5) Yang, K.; Zhang, S.; Zhang, G.; Sun, X.; Lee, S.-T.; Liu, Z. *Nano Lett.* **2010**, *10*, 3318.
(6) Huang, X. Q.; Tang, S. H.; Mu, X. L.; Dai, Y.; Chen, G. X.; Zhou, Z. Y.; Ruan, F. X.; Yang, Z. L.; Zheng, N. F. *Nat. Nanotechnol.* **2011**, *6*, 28.
(7) Hessel, C. M.; P. Pattani, V.; Rasch, M.; Panthani, M. G.; Koo, B.; Tunnell, J. W.; Korgel, B. A. *Nano Lett.* **2011**, *11*, 2560.
(8) Tian, Q.; Jiang, F.; Zou, R.; Liu, Q.; Chen, Z.; Zhu, M.; Yang, S.; Wang, J.; Wang, J.; Hu, J. *ACS Nano* **2011**, *5*, 9761.
(9) Tian, Q.; Tang, M.; Sun, Y.; Zou, R.; Chen, Z.; Zhu, M.; Yang, S.; Wang, J.; Wang, J.; Hu, J. *Adv. Mater.* **2011**, *23*, 3542.
(10) Zhou, M.; Zhang, R.; Huang, M.; Lu, W.; Song, S.; Melancon, M. P.; Tian, M.; Liang, D.; Li, C. *J. Am. Chem. Soc.* **2010**, *132*, 15351.
(11) Li, Y.; Lu, W.; Huang, Q.; Li, C.; Chen, W. *Nanomedicine* **2010**, *5*, 1161.
(12) Alvarez-Lorenzo, C.; Bromberg, L.; Concheiro, A. *Photochem. Photobiol.* **2009**, *85*, 848.
(13) Le Duc, G.; Miladi, I.; Alric, C.; Mowat, P.; Bräuer-Krisch, E.; Bouchet, A.; Khalil, E.; Billotey, C.; Janier, M.; Lux, F.; Epicier, T.; Perriat, P.; Roux, S.; Tillement, O. *ACS Nano* **2011**, *5*, 9566.
(14) Jain, S.; Hirst, D. G.; O'Sullivan, J. M. *Br. J. Radiol.* **2012**, *85*, 101.
(15) Chang, M.-Y.; Shiau, A.-L.; Chen, Y.-H.; Chang, C.-J.; Chen, H. H. W.; Wu, C.-L. *Cancer Sci.* **2008**, *99*, 1479.
(16) Jain, S.; Coulter, J. A.; Hounsell, A. R.; Butterworth, K. T.; McMahon, S. J.; Hyland, W. B.; Muir, M. F.; Dickson, G. R.; Prise, K. M.; Currell, F. J.; O'Sullivan, J. M.; Hirst, D. G. *Int. J. Radiat. Oncol.* **2011**, *79*, 531.
(17) Prezado, Y.; Fois, G.; Le Duc, G.; Bravin, A. *Med. Phys.* **2009**, *36*, 3568.
(18) Kobayashi, K.; Usami, N.; Porcel, E.; Lacombe, S.; Le Sech, C. *Mutat. Res.-Rev. Mutat. Res.* **2010**, *704*, 123.
(19) Chithrani, D. B.; Jelveh, S.; Jalali, F.; van Prooijen, M.; Allen, C.; Bristow, R. G.; Hill, R. P.; Jaffray, D. A. *Radiat. Res.* **2010**, *173*, 719.
(20) Liu, Y.; Ai, K.; Liu, J.; Yuan, Q.; He, Y.; Lu, L. *Angew. Chem., Int. Ed.* **2012**, *51*, 1437.
(21) Xing, H.; Bu, W.; Ren, Q.; Zheng, X.; Li, M.; Zhang, S.; Qu, H.; Wang, Z.; Hua, Y.; Zhao, K.; Zhou, L.; Peng, W.; Shi, J. *Biomaterials* **2012**, *33*, 5384.
(22) Gerweck, L. E.; Gillette, E. L.; Dewey, W. C. *Radiat. Res.* **1975**, *64*, 611.
(23) Overgaard, J.; Bichel, P. *Radiology* **1977**, *123*, 511.
(24) Horsman, M. R.; Overgaard, J. *Clin. Oncol.-UK* **2007**, *19*, 418.
(25) Benhur, E.; Elkind, M. M.; Bronk, B. V. *Radiat. Res.* **1974**, *58*, 38.
(26) Chen, G.; Shen, J.; Ohulchanskyy, T. Y.; Patel, N. J.; Kutikov, A.; Li, Z.; Song, J.; Pandey, R. K.; Ågren, H.; Prasad, P. N.; Han, G. *ACS Nano* **2012**, *6*, 8280.
(27) Wang, F.; Liu, X. *Chem. Soc. Rev.* **2009**, *38*, 976.
(28) Zhou, J.; Liu, Z.; Li, F. *Chem. Soc. Rev.* **2012**, *41*, 1323.
(29) Nyk, M.; Kumar, R.; Ohulchanskyy, T. Y.; Bergey, E. J.; Prasad, P. N. *Nano Lett.* **2008**, *8*, 3834.
(30) Cheng, L.; Yang, K.; Li, Y.; Chen, J.; Wang, C.; Shao, M.; Lee, S.-T.; Liu, Z. *Angew. Chem., Int. Ed.* **2011**, *50*, 7385.
(31) Xing, H.; Bu, W.; Zhang, S.; Zheng, X.; Li, M.; Chen, F.; He, Q.; Zhou, L.; Peng, W.; Hua, Y.; Shi, J. *Biomaterials* **2012**, *33*, 1079.
(32) Ku, G.; Zhou, M.; Song, S.; Huang, Q.; Hazle, J.; Li, C. *ACS Nano* **2012**, *6*, 7489.
(33) Fong, P. M.; Keil, D. C.; Does, M. D.; Gore, J. C. *Phys. Med. Biol* **2001**, *46*, 3105.
(34) Hauck, T. S.; Jennings, T. L.; Yatsenko, T.; Kumaradas, J. C.; Chan, W. C. W. *Adv. Mater.* **2008**, *20*, 3832.
(35) Suit, H. D.; Gerweck, L. E. *Cancer Res.* **1979**, *39*, 2290.
(36) Wang, C.; Tao, H.; Cheng, L.; Liu, Z. *Biomaterials* **2011**, *32*, 6145.
(37) Fischer, L. H.; Harms, G. S.; Wolfbeis, O. S. *Angew. Chem., Int. Ed.* **2011**, *50*, 4546.
(38) Idris, N. M.; Gnanasammandhan, M. K.; Zhang, J.; Ho, P. C.; Mahendran, R.; Zhang, Y. *Nat. Med.* **2012**, *18*, 1580.
(39) Jayakumar, M. K. G.; Idris, N. M.; Zhang, Y. *Proc. Natl. Acad. Sci. U.S.A.* **2012**, *109*, 8483.
(40) Liu, J.; Bu, W.; Pan, L.; Shi, J. *Angew. Chem., Int. Ed.* **2013**, *52*, 4375.
(41) Yang, Y.; Shao, Q.; Deng, R.; Wang, C.; Teng, X.; Cheng, K.; Cheng, Z.; Huang, L.; Liu, Z.; Liu, X.; Xing, B. *Angew. Chem., Int. Ed.* **2012**, *51*, 3125.
(42) Yan, B.; Boyer, J.-C.; Habault, D.; Branda, N. R.; Zhao, Y. *J. Am. Chem. Soc.* **2012**, *134*, 16558.